Homogeneous Quasi-Geostrophic Turbulence Driven by a Uniform Temperature Gradient

DALE B. HAIDVOGEL

Department of Physical Oceanography, Woods Hole Oceanographic Institution, Woods Hole, MA 02543

ISAAC M. HELD

Geophysical Fluid Dynamics Laboratory/NOAA, Princeton University, Princeton, NJ 08540

(Manuscript received 24 March 1980, in final form 2 September 1980)

ABSTRACT

Statistically steady states consistent with a horizontally uniform time-averaged temperature gradient in a two-layer quasi-geostrophic model on a beta-plane are found by numerically integrating the equations for deviations from this mean state in a doubly periodic domain. Based on the result that the flow statistics are not strongly dependent on the size of the domain, it is suggested that this homogeneous flow is physically realizable. The dependence of the eddy heat and potential vorticity fluxes and eddy energy level on various model parameters (the beta effect, surface drag, small-scale horizontal mixing) is described. Implications for eddy flux parameterization theories are discussed.

1. Introduction

Most turbulent transport problems are fundamentally inhomogeneous. In a typical laboratory turbulent shear flow, for example, momentum mixing is predominantly due to eddies with scales comparable to the width of the shear zone (see, e.g., Tennekes and Lumley, 1972). In turbulent Bénard convection, the eddies carrying most of the heat are effectively "plumes" extending from one boundary of the unstable region to the other. In both problems, the scale of the eddies responsible for the bulk of the transport is determined by the scale of the mean flow inhomogeneity in the direction of the transport. This absence of scale separation is the principal source of difficulty in constructing plausible theories for turbulent mixing.

Fortunately, horizontal eddy heat and potential vorticity fluxes in a turbulent quasi-geostrophic flow may not be fundamentally inhomogeneous in this sense (although particular problems of interest may be inhomogeneous, of course). We argue below that when the mean flow variations in the horizontal are small over a Rossby radius of deformation (λ) then λ asserts itself as the appropriate "mixing length," or characteristic horizontal scale, of the eddies transporting heat and potential vorticity. The resulting scale separation has considerable significance for the effect of the eddy fluxes on the mean flow and, particularly important for our purposes, allows one to pose a physically meaningful horizontally homogeneous problem.

To clarify the difference between problems that are fundamentally inhomogeneous and those that are not, compare the quasi-geostrophic problem depicted schematically in Figs. 1a and 1b with the Bénard convection problem in Figs. 1c and 1d. In the quasi-geostrophic case, it is assumed that: 1) potential temperatures relax to a given profile $\theta_E(y,z)$ in the absence of a dynamical heat flux; 2) the meridional gradient of θ_E is constant within a region of width L and zero outside of this region; 3) the flow consistent with these temperatures is unstable; and 4) the dynamical fluxes in the resulting statistically steady state produce the time-averaged profiles shown as dotted lines in the figures. A flow for which $\lambda \approx L (\lambda \ll L)$ is illustrated in Fig. 1a (Fig. 1b). In the latter case, we do not expect eddy statistics near the center of the unstable region to be greatly influenced by boundary effects, as long as these eddies are indeed typically of scale $\lambda \ll L$. Accordingly, eddy statistics close to the center should be nearly homogeneous, the divergence of the heat flux should be small, and θ should be close to θ_E, as shown in the figure. Letting L approach infinity while holding $\partial\theta_E/\partial y$ fixed, we expect that the transient eddy statistics will reduce to those of a horizontally homogeneous flow driven by an imposed time-mean temperature gradient.

We do not mean to imply in Fig. 1b that λ itself is necessarily a good measure of the distance from the boundary of the unstable region to which the eddy effects on the mean flow penetrate. This pene-

0022-4928/80/122644-17$08.25

tration distance depends on other model parameters as well, particularly the time scale on which θ relaxes to θ_E in the absence of dynamical fluxes (see the discussion in Section 6 below). We do expect, however, that this penetration distance will become a smaller and smaller fraction of L, the width of the unstable region, as $L \to \infty$ while holding $\partial\theta_E/\partial y$ and all other parameters fixed.

In the analogous problem for Bénard convection, a fluid layer of depth H relaxes to an unstable stratification $\theta_E(z)$ in the absence of dynamical fluxes. Once again, the question of interest is whether or not the resulting turbulent flow field near the center of the unstable region tends toward homogeneity as H is increased, holding $\partial\theta_E/\partial z$ fixed. In fact, it is well known from laboratory, observational and theoretical studies that homogeneity will not be approached. Instead, the eddies increase in size as the size of the unstable region increases. As a result, the eddies carrying heat through the center of the unstable layer are sensitive to the total potential temperature drop across the layer, their structure having little to do with the local gradient of θ_E. To a first approximation, one expects $\partial\theta/\partial z \approx 0$ as shown in Figs. 1c and 1d, rather than $\partial\theta/\partial z \approx \partial\theta_E/\partial z$. In contrast to the quasi-geostrophic example, the problem of homogeneous turbulence driven by a uniform unstable stratification is unphysical, a result attributable to the absence of a scale analogous to λ.

In order to study the homogeneous limit of the quasi-geostrophic problem, one could analyze the flow pictured in Fig. 1b, concentrating on the statistics near the center of the unstable region. However, to make the computational problem more manageable and the analysis more straightforward, we proceed instead by assuming that the time-averaged flow is horizontally uniform and then solving for the forced transient flow field in a doubly periodic box. As a result, the transient eddy statistics are automatically horizontally homogeneous in the domain of integration. We assume as a working hypothesis that if the homogeneous problem is not physically meaningful then either 1) a statistically steady state will not exist, or more likely, 2) the dependence of the eddy statistics on the size L of the doubly periodic box will not disappear as $(\lambda/L) \to 0$. If the eddy statistics do asymptote to finite values in this limit, it is then reasonable to assume that the reentrant boundary conditions do not matter and that the statistics in this limit are, in fact, identical with those in the interior of the unstable flow of Fig. 1b in the same limit $[(\lambda/L) \to 0]$.

We describe in this paper a series of calculations with a two-layer quasi-geostrophic model on a beta-plane (Phillips, 1951; Pedlosky, 1963), limiting the discussion to the special case of layers of equal depth. In the most general homogeneous problem

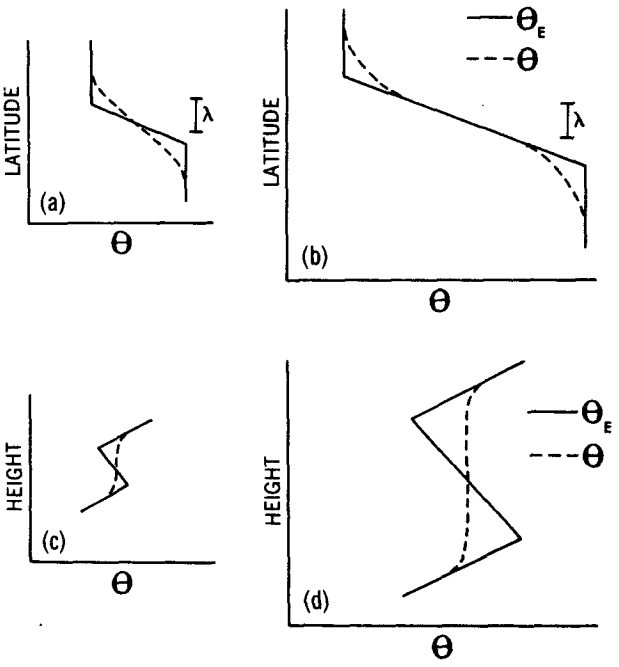

FIG. 1. A schematic of the effects of quasi-geostrophic eddies on mean potential temperature as a function of latitude, $\theta(y)$, in a baroclinically unstable flow (a and b), and the effects of turbulent convection on mean potential temperature as a function of height, $\theta(z)$, in an unstably stratified flow (c and d). θ_E is the potential temperature in the absence of dynamical fluxes. As the width of the unstable region in the quasi-geostrophic case increases ($a \to b$), we argue that θ approaches θ_E away from the boundaries of the unstable region. This does not occur as the size of the unstable region increases in the case of turbulent convection ($c \to d$).

the mean temperature gradient need not be directed parallel to the planetary vorticity gradient, but we restrict ourselves here to the simplest case of a north-south temperature gradient (or zonal mean wind shear).

After presenting the model equations in Section 2, we proceed to demonstrate in Section 3 that for a certain range of model parameters the transient eddy statistics are only weakly dependent on the size of the doubly periodic computational domain. The dependence of the homogeneous statistics on the various nondimensional model parameters is then examined by selecting a pivot experiment and varying each parameter individually about this pivot. The pivot experiment is described in Section 4 and the parameter variations in Section 5.

We focus in particular on the dependence of the time-averaged heat (or buoyancy) flux through the system on the various model parameters. The mean eddy potential vorticity fluxes, the mean eddy energy generation, and the mean eddy potential enstrophy generation (in either layer) are all simply proportional to the heat flux in this horizontally homogeneous quasi-geostrophic system. Some

implications of these results for eddy flux closure schemes are discussed in Section 6.

A fundamental characteristic of quasi-geostrophic flows on a beta-plane is that the energy, once cascaded to large horizontal scales, organizes itself into zonal jets (Rhines, 1977; Williams, 1978). Transient zonal jets are, indeed, generated in these homogeneous calculations, but we postpone to a later paper an analysis of their formation and maintenance.

We have chosen to describe and compare a large number of experiments rather than analyze any single experiment in great detail. In particular, no detailed comparison of these results with the predictions of turbulent closure theories is attempted. In both of these respects, the recent work of Salmon (1977, 1980) on essentially the same dynamical system is complementary to ours.

2. The physical and numerical models

In dimensional form, the equations of motion for a flat-bottom quasi-geostrophic two-layer model on a beta-plane can be written

$$\frac{\partial Q_1}{\partial t} + J(\Psi_1,Q_1) = -\nu\nabla^6\Psi_1, \tag{1a}$$

$$\frac{\partial Q_2}{\partial t} + J(\Psi_2,Q_2) = -\nu\nabla^6\Psi_2 - \kappa\nabla^2\Psi_2, \tag{1b}$$

where the subscripts 1 and 2 refer to the upper and lower layers respectively, J is the horizontal Jacobian and ∇^2 the horizontal Laplacian operator. The two layers are assumed to have equal depths when at rest. The potential vorticities, Q_i, and the velocities (u_i,v_i), are related to the streamfunctions Ψ_i through the diagnostic relations

$$\left.\begin{aligned} Q_1 &= \nabla^2\Psi_1 + \beta y + \frac{1}{2\lambda^2}(\Psi_2 - \Psi_1) \\ Q_2 &= \nabla^2\Psi_2 + \beta y + \frac{1}{2\lambda^2}(\Psi_1 - \Psi_2) \\ (u_i,v_i) &= (-\partial\Psi_i/\partial y,\ \partial\Psi_i/\partial x), \quad i = 1, 2 \end{aligned}\right\}.$$

In these equations λ is the Rossby radius of deformation, $\lambda \equiv [g'H/2f_0^2]^{1/2}$, where H is the resting depth of either layer, g' is the reduced gravity $[g' = g(\rho_2 - \rho_1)/\rho_1]$, and f_0 is the Coriolis parameter evaluated at some central latitude. The upward displacement η of the interface between the two layers is given by $f_0\eta/H = (1/2\lambda^2)(\Psi_2 - \Psi_1)$.

Eqs. (1a) and (1b) state that upper and lower layer potential vorticity are conserved following the horizontal flow, except for the effects of dissipative processes. These latter processes are assumed to act on the relative vorticity $(\nabla^2\Psi_i)$ through a biharmonic lateral diffusion ($i = 1, 2$) and a linear surface drag ($i = 2$ only) with turbulent mixing coefficients ν and κ, respectively. The use of this mixed dissipative parameterization follows recent practice, particularly in oceanographic modeling (see, e.g., Bretherton and Haidvogel, 1976; Holland, 1978). The scale-selective lateral dissipative term is intended to mimic the removal of enstrophy on scales of motion unresolved by the finite computational grid (to be discussed below). The biharmonic form of this horizontal mixing is somewhat arbitrary. Although some scale-selective mixing is required to regulate the accumulation of enstrophy at the highest allowable wavenumbers, the typical expectation is that the statistics of the large-scale flow will not be sensitive to the choice of the coefficient ν. (This assumption will be critically examined below.) The form of the surface drag, on the other hand, does have some justification (Ekman pumping), and one expects the strength of this drag to affect the energy level of the large-scale flow.

Following our discussion in the Introduction, we assume that our turbulent fluid is characterized by a horizontally uniform time-averaged temperature gradient (directed north-south). Equivalently, the time-averaged vertical shear is horizontally uniform and zonal. For definiteness, the mean velocity (U) is confined to the upper layer, so that

$$\left.\begin{aligned} \Psi_1(x,y,t) &= -Uy + \psi_1(x,y,t) \\ \Psi_2(x,y,t) &= \psi_2(x,y,t) \end{aligned}\right\},$$

where $\psi_i (i = 1, 2)$ is the deviation of the streamfunction from its time average. Nondimensionalizing (x,y,t,ψ) by $(\lambda,\lambda,\lambda/U,U\lambda)$, the quasi-geostrophic potential vorticity equations for the transient flow become

$$\frac{\partial q_1}{\partial t} + J(\psi_1,q_1) = -\hat{\nu}\nabla^6\psi_1 + F_1, \tag{2a}$$

$$\frac{\partial q_2}{\partial t} + J(\psi_2,q_2) = -\hat{\nu}\nabla^6\psi_2 - \hat{\kappa}\nabla^2\psi_2 + F_2, \tag{2b}$$

where the eddy potential vorticities are

$$q_1 \equiv \nabla^2\psi_1 + \tfrac{1}{2}(\psi_2 - \psi_1), \tag{3a}$$

$$q_2 \equiv \nabla^2\psi_2 + \tfrac{1}{2}(\psi_1 - \psi_2). \tag{3b}$$

The forcing terms

$$F_1 \equiv -\frac{\partial q_1}{\partial x} - (\hat{\beta} + \tfrac{1}{2})\frac{\partial\psi_1}{\partial x}, \tag{4a}$$

$$F_2 \equiv -(\hat{\beta} - \tfrac{1}{2})\frac{\partial\psi_2}{\partial x}, \tag{4b}$$

represent the effects of the mean temperature and planetary vorticity gradients on the transient flow. All variables in Eqs. (2)–(4) and in all subsequent equations—unless otherwise noted—are nondi-

mensional. The parameters which appear in these equations are $\hat{\beta} \equiv \beta\lambda^2/U$, $\hat{\kappa} \equiv \kappa\lambda/U$ and $\hat{\nu} \equiv \nu/\lambda^3 U$.

With the assumption of horizontal homogeneity, we require that $\psi_i(x,y,t)$, $i = 1, 2$ be periodic over the square domain $0 \leq x, y \leq 2\pi\hat{L}$, where $\hat{L} \equiv L/\lambda$, $2\pi L$ being the dimensional size of the domain. Adopting the spectral approximation method, we set

$$\psi_i(x,y,t) = \sum_{m=-N/2}^{N/2-1} \sum_{n=-N/2}^{N/2-1} A^i_{mn}(t) e^{i(k_m x + l_n y)}, \quad i = 1, 2, \tag{5}$$

where

$$A^i_{-m,-n}(t) = [A^i_{mn}(t)]^*,$$

$$(k_m, l_n) = (m,n)/\hat{L},$$

Note that the largest wavenumber retained in the numerical model, $k_{\max} = (N/2\hat{L})$. Substitution into (2a,b) yields a coupled set of equations for the evolution of the spectral coefficients $A^i_{mn}(t)$. These equations are advanced in time using a leapfrog differencing scheme, with periodic application of a leapfrog-trapezoidal step (Haltiner, 1971) to diminish the computational mode. The nonlinear products $J(\psi_i, q_i)$ are computed without aliasing error using the transform method (Orszag, 1971).

The resulting physical/computational problem is characterized by five nondimensional parameters of potential interest. Only two of these—$\hat{\beta}$ and $\hat{\kappa}$—are associated with the physical description of the problem, being nondimensional measures of the planetary vorticity gradient and bottom friction. Three others—$\hat{L}$, $k_{\max}$ and $\hat{\nu}$—are considered computational; they reflect the computational requirements of a finite domain size and horizontal resolution, and of a mechanism for enstrophy removal from the high-wavenumber end of the discrete spectrum. Our hope is to achieve statistically steady states independent of domain size, grid size, and subgridscale dissipative mechanism. In all of the experiments described below, $N = 64$; therefore, the nondimensional box size ($2\pi\hat{L}$) and the nondimensional grid size ($2\pi k_{\max}^{-1}$) are not varied independently, a point we return to in Section 3. We also neglect the computational parameters associated with the temporal resolution of the numerical model. The nondimensional time step in the following calculations (typically $\Delta t = 0.025$) has been chosen to avoid numerical instability and to ensure negligibly small time truncation errors.

From the potential vorticity equations (2a,b), the globally-averaged energy and enstrophy budget equations can be constructed. These are

$$\frac{\partial E}{\partial t} = \frac{\partial}{\partial t}[\tfrac{1}{2}(K_1 + K_2) + P] = \frac{\partial}{\partial t}(E_{BT} + E_{BC}) = G + S + D, \tag{6a}$$

$$\frac{\partial p_1}{\partial t} = g_1 + d_1, \tag{6b}$$

$$\frac{\partial p_2}{\partial t} = g_2 + s + d_2, \tag{6c}$$

where

$$K_i \equiv \tfrac{1}{2}\langle |\nabla\psi_i|^2 \rangle, \quad (i = 1, 2),$$

$$P \equiv \frac{1}{2}\left\langle \left(\frac{\psi_1 - \psi_2}{2}\right)^2 \right\rangle,$$

$$E_{BT} \equiv \frac{1}{2}\left\langle \left| \nabla\left(\frac{\psi_1 + \psi_2}{2}\right)\right|^2 \right\rangle,$$

$$E_{BC} \equiv \frac{1}{2}\left\langle \left| \nabla\left(\frac{\psi_1 - \psi_2}{2}\right)\right|^2 + \left(\frac{\psi_1 - \psi_2}{2}\right)^2 \right\rangle,$$

$$G \equiv \frac{1}{2}\left\langle \psi_1 \frac{\partial q_1}{\partial x} \right\rangle,$$

$$S \equiv -\frac{\hat{\kappa}}{2}\langle |\nabla\psi_2|^2 \rangle,$$

$$D \equiv -\frac{\hat{\nu}}{2}\langle |\nabla(\nabla^2\psi_1)|^2 + |\nabla(\nabla^2\psi_2)|^2 \rangle,$$

$$p_i \equiv \langle |q_i| \rangle^2, \quad (i = 1, 2),$$

$$g_1 \equiv -2(\hat{\beta} + \tfrac{1}{2})\left\langle q_1 \frac{\partial\psi_1}{\partial x} \right\rangle,$$

$$g_2 \equiv -2(\hat{\beta} - \tfrac{1}{2})\left\langle q_2 \frac{\partial\psi_2}{\partial x} \right\rangle,$$

$$d_i \equiv -2\hat{\nu}\langle q_1 \nabla^6 \psi_i \rangle, \quad (i = 1, 2),$$

$$s \equiv -2\hat{\kappa}\langle q_2 \nabla^2 \psi_2 \rangle.$$

In these expressions, brackets indicate a global average. The total energy E—consisting of upper layer kinetic (K_1), lower layer kinetic (K_2), and potential (P) energies; or, alternatively, of energy in the barotropic (E_{BT}) and baroclinic (E_{BC}) modes—varies in time as a result of net generation (G) and net loss due to surface friction (S) and lateral viscous processes (D). Eqs. (6b) and (6c) express similar balances for the upper and lower layer potential enstrophies, p_1 and p_2. It is important to realize that G, g_1, and g_2 are all proportional to each other and to the eddy heat flux through the system; in particular,

$$\left\langle \psi_1 \frac{\partial q_1}{\partial x} \right\rangle = -\left\langle q_1 \frac{\partial\psi_1}{\partial x} \right\rangle = -\frac{1}{2}\left\langle \psi_2 \frac{\partial\psi_1}{\partial x} \right\rangle = \left\langle q_2 \frac{\partial\psi_2}{\partial x} \right\rangle = \frac{1}{2}\left\langle \psi_1 \frac{\partial\psi_2}{\partial x} \right\rangle = -\left\langle \left(\frac{\psi_2 - \psi_1}{2}\right)\frac{\partial}{\partial x}\left(\frac{\psi_1 + \psi_2}{2}\right) \right\rangle, \tag{7}$$

the last expression being proportional to the heat (or buoyancy) flux.

We shall have occasion to refer not only to the domain averages of several of the terms in Eqs. (6a,b,c), but to their one- and two-dimensional spectra as well. Our normalization conventions and notation for these spectra are listed in Appendix A.

A total of 37 statistically steady states have been obtained with this model, providing very modest coverage of the parameter space. Each experiment is initiated from a randomly chosen set of spectral coefficients A^i_{mn} ($i = 1, 2$). After an initial period of integration lasting 100–200 advective times, the system appears to reach statistical equilibrium. (The eddy generation and energy invariably overshoot the final average values during this spin-up, sometimes quite dramatically.) Subsequent to this equilibration, an additional integration of several hundred advective times is performed to provide time-averaged flow statistics. A table in Appendix B summarizes some of the properties of the statistically steady states thus obtained.

An attempt has been made to estimate sampling errors by splitting the averaging interval into $M = 10$–20 subintervals, computing the variances of the subaverages, and then dividing by M to obtain an estimate of the variances of averages over the full interval. The resulting estimates of the standard deviation of domain-averaged energy generation or total energy were typically O(2–5%) of the mean values. Since successive averages over the subintervals were occasionally strongly positively correlated, this is only a lower bound on possible sampling errors. Inspection of the solutions reveals the occasional presence of very long-period variations in the energy of the largest waves in the system, making it unlikely that convincing estimates of sampling errors can be obtained without much longer integrations. The results described in the following section—particularly those achieved by varying $\hat{L}$ and $\hat{\nu}$ by small amounts (see Fig. 2a,b)—suggest that our sampling errors are occasionally O(10%).

3. The radius of deformation as mixing length

It is not self-evident that the meridional scale of the eddies transporting heat and potential vorticity in this problem, in fact, will be determined by the radius of deformation alone. Linear instability theory generally predicts the largest growth rates at zonal scales comparable to λ; however, the meridional scale of the most unstable wave can be much larger (Simmons, 1974). In our horizontally homogeneous problem, the most unstable wave on the time-averaged flow has no meridional structure (i.e., $l = 0$). It might therefore be argued that the $l = 0$ mode must dominate the flow. However, although our mean flow is most unstable to single wave disturbances of infinite meridional extent, it can be shown (Pedlosky, 1975) that the marginally stable mode at the minimum critical shear required for instability is itself unstable to motions whose meridional scale is O(λ). More generally, if the flow is at all turbulent one expects nonlinear interactions to force the system toward isotropy, impressing the characteristic zonal scale of the generation process on meridional variations as well. We test this intuition by examining the dependence of time-averaged flow statistics on the parameter $\hat{L} = L/\lambda$.

As stated in Section 2, $(k_{\max}\hat{L})$ is fixed in all of our experiments. When $\hat{L}$ is altered, holding the radius of deformation fixed, then $k_{\max}$ is correspondingly altered. To help separate the different effects of finite domain size and finite resolution when $\hat{L}$ is varied, it is useful to examine the behavior of the system in the $\hat{\nu} - \hat{L}$ plane, since the effects of finite resolution are expected to be sensitive to $\hat{\nu}$.

Figs. 2a and 2b depict the time and domain-averaged energy generation G and total eddy energy E obtained for a number of values of $\hat{\nu}$ and $\hat{L}$, with $\hat{\beta} = 0.25$ and $\hat{\kappa} = 0.5$. A clear feature in this figure at the smaller values of $\hat{\nu}$ is the rapid decrease in G that eventually occurs as $\hat{L}$ increases at fixed $\hat{\nu}$. The corresponding decrease in E is somewhat less clear. This decrease is evidently associated with inadequate resolution since the value of $\hat{L}(k_{\max})$ at which this transition occurs decreases (increases) with decreasing $\hat{\nu}$. Although the small number of experiments does not allow us to be at all precise, the results are not inconsistent with the intuitive idea that severe distortion of the solution occurs when the parameter

$$R^{1/3} \equiv 1/(k_{\max}\hat{\nu}^{1/3})$$

rises substantially above a critical value (≈ 4). Here R is an effective Reynolds number for the smallest wave in the system, if velocities are of order unity. (Fig. 2b shows that rms velocities are indeed of order unity for this choice of $\hat{\beta}$ and $\hat{\kappa}$.)

If we disregard this rapid drop-off when the resolution is inadequate, these results suggest that the generation (or the heat flux) and the energy level are not particularly sensitive to $\hat{L}$. As $\hat{L}$ is decreased, one does expect distortion due to quantization of **k**-space to become evident eventually, but Fig. 2 indicates that the effect on G and E is rather small and not entirely systematic, at least down to $\hat{L} = 7$. The only systematic variation we find in the $\hat{\nu}$-$\hat{L}$ plane, besides that attributed to inadequate resolution, is a significant decrease in G and E with increasing $\hat{\nu}$ for $\hat{\nu} \geq 0.2$. The region in the $\hat{\nu}$-$\hat{L}$ plane within which resolution is adequate, and $\hat{\nu}$ sufficiently small that it does not affect G and E significantly, is evidently quite small for this model. A model with a larger number of degrees of

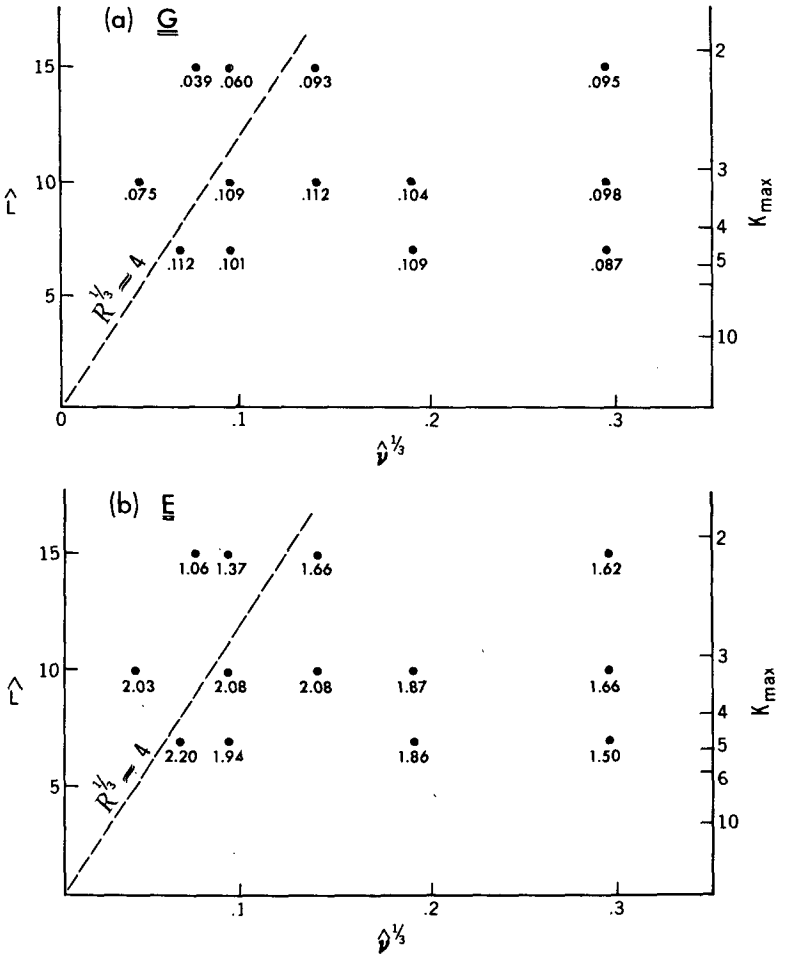

FIG. 2. The domain averaged eddy energy generation G and total eddy energy E as functions of $\hat{\nu}$ and $\hat{L}$ (or k_{max}) with $\hat{\beta} = 0.25$ and $\hat{\kappa} = 0.5$. R, effectively the Reynolds number for the smallest wave in the system, is defined in the text.

freedom seems to be required in order to obtain more satisfactory results.

Two of these experiments—($\hat{L} = 10, \nu^{1/3} = 0.292$) and ($\hat{L} = 15, \hat{\nu}^{1/3} = 0.292$) are compared in greater detail in Figs. 3–6. These experiments, conducted at relatively high values of $\hat{\nu}$ and $\hat{L}$, are the pair most likely to show $\hat{L}$-independent behavior, being rather far removed from regions in the $\hat{\nu}$-$\hat{L}$ plane where one expects finite resolution and finite domain size to be strongly felt. Plotted in Fig. 3 are the one-dimensional zonal and meridional energy generation spectra, $G(k)$ and $G(l)$. The spectra in the two experiments are nearly identical; there is, in particular, no noticeable shift in the zonal or meridional scale of the eddies transporting heat and no significant change in the total heat flux. (The fact that the generation peaks at or near $l = 0$ should not raise concern as to the physical realizeability of the flow. Fig. 3 suggests that $\lim G(l)$ as $\hat{L} \to \infty$ does exist for all l, including $l = 0$. If this is the case, then for sufficiently large $\hat{L}$ an arbitrarily small fraction of the generation occurs on scales larger than any fixed fraction of the domain width.) Fig. 4, a plot of zonal spectra of the eddy energy in the barotropic and baroclinic modes, further illustrates this similarity. Not only are the details of the energy spectra similar on scales considerably smaller than the domain size, as one might expect, but the amount of eddy energy that accumulates in the $k = 0$ mode is also nearly identical in the two cases.

Closer inspection of these transient zonal jets does, however, reveal a significant difference between the two experiments; the meridional scale of the jets is more sharply defined in the $\hat{L} = 15$ than in the $\hat{L} = 10$ calculation. Fig. 5 is a plot of $E(k = 0, l)$ for the two experiments. Both spectra have a peak at $l \approx 0.5$, and both have about the same total energy under the peak (see Fig. 4) but the peak is much sharper for $\hat{L} = 15$ than for $\hat{L} = 10$. It

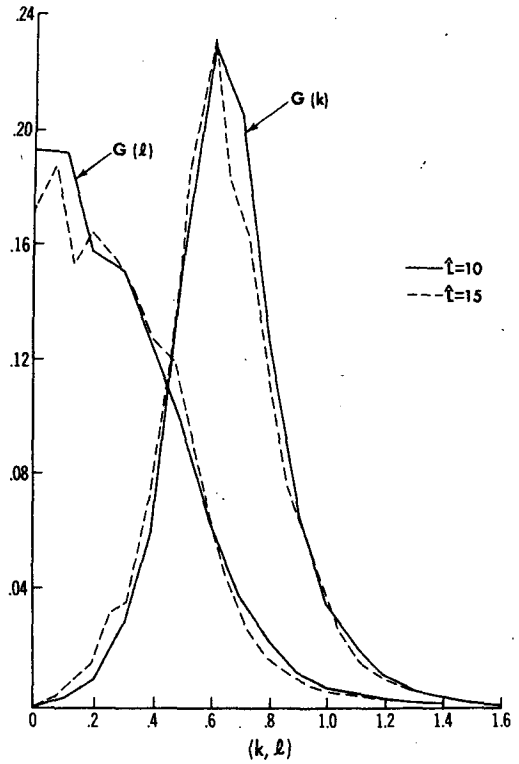

FIG. 3. The zonal $G(k)$ and meridional $G(l)$ energy generation spectra for the experiments $\hat{L} = 15$, $\hat{\nu}^{1/3} = 0.292$, $\hat{\beta} = 0.25$, $\hat{\kappa} = 0.5$ (dotted line) and $\hat{L} = 10$, $\hat{\nu}^{1/3} = 0.292$, $\hat{\beta} = 0.25$, $\hat{\kappa} = 0.5$ (solid line).

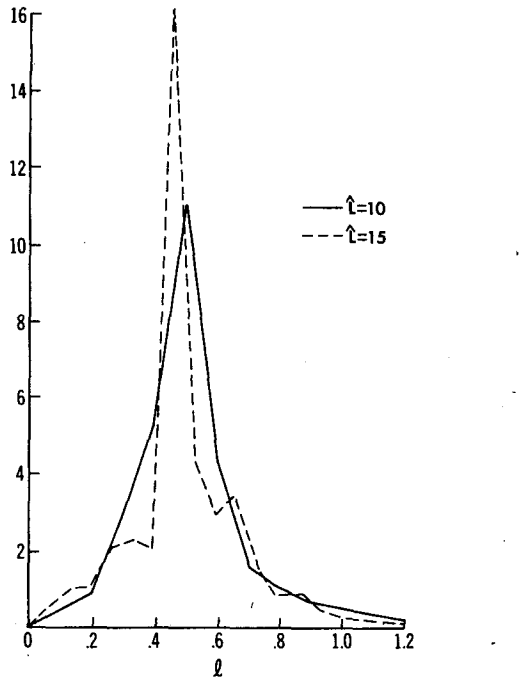

FIG. 5. The total eddy energy in the $k = 0$, or zonally symmetric, flow as a function of the meridional wavenumber for the same two experiments as in Fig. 3.

seems that the width of the peak is limited by the resolution in wavenumber space. (When we repeat this calculation with $\hat{L} = 7$, we find that $E(0,l)$ has no prominent peak at all.) This is the only difference we find between these two experiments that

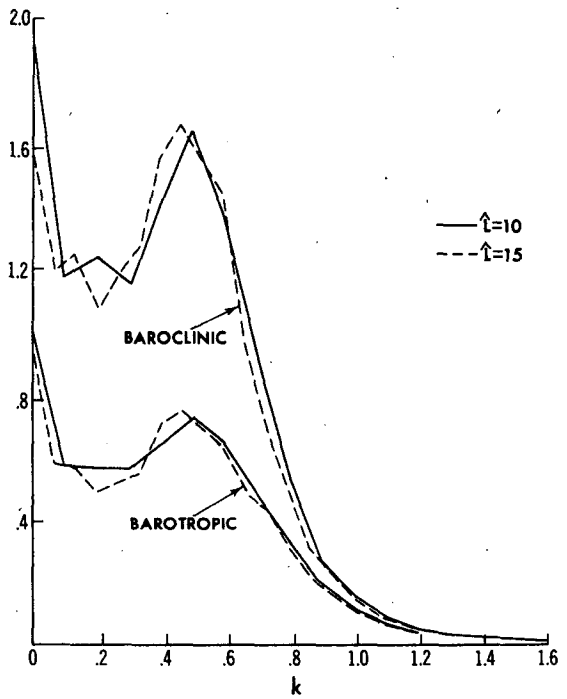

FIG. 4. The zonal spectra of the eddy energy in the barotropic $[E_{BT}(k)]$ and baroclinic $[E_{BC}(k)]$ modes for the same two experiments as in Fig. 3.

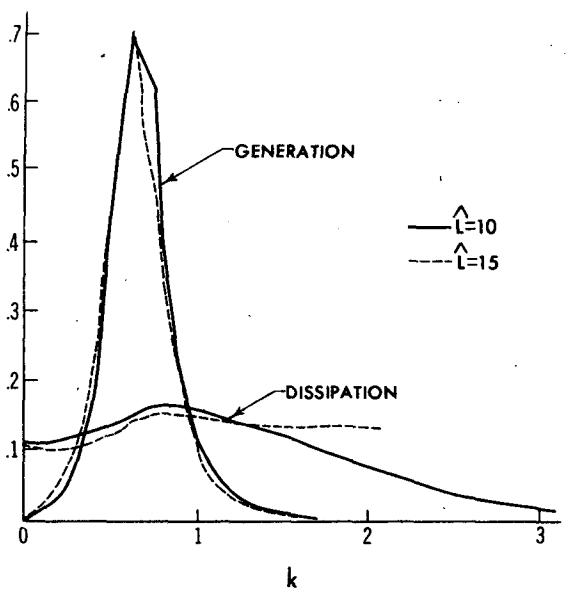

FIG. 6. Zonal spectra of the potential enstrophy generation $g_1(k)$ and dissipation $d_1(k)$ in the upper layer for the same two experiments as in Fig. 3.

is clearly attributable to finite domain size. We expect that if $\hat{L}$ were sufficiently large that the model's resolution in wavenumber space were sufficient to resolve the natural width of this spectral peak, then the structure of the peak would no longer change if $\hat{L}$ were increased further.

On the smallest scales, some differences between these two numerical experiments also exist, presumably due to insufficient resolution. Fig. 6 contains plots of the zonal spectra of the potential enstrophy generation $g_1(k)$ and dissipation $d_1(k)$ in the model's upper layer. (The lower layer enstrophy balance is complicated by surface drag.) The enstrophy dissipation is clearly not as well resolved in the $\hat{L} = 15$ as in the $\hat{L} = 10$ case, but there is little apparent effect on the generation process. Thus, despite differences at the largest scales due to finite domain size and at the smallest scales due to finite grid size, eddy statistical properties such as net eddy heat flux appear to scale with the radius of deformation to a good approximation. We tentatively conclude that this homogeneous problem is indeed physically meaningful.

The two experiments discussed above are both fairly viscous. A substantial fraction (30%) of the dissipation of kinetic energy is accounted for by the horizontal mixing. Fig. 2 also seems to show a small but systematic increase in G and E with decreasing $\hat{\nu}$ at these large values of the viscosity. Because of the arbitrary character of this subgrid-scale mixing, it is desirable to conduct most of our experiments at a smaller value of $\hat{\nu}$ so that: 1) the bulk of the eddy kinetic energy is dissipated by surface drag, and 2) the effect of $\hat{\nu}$ on the generation is as small as possible. Fig. 7 shows the zonal spectra of the upper level enstrophy generation $g_1(k)$ and dissipation, $d_1(k)$, for experiments with $\hat{L} = 10$ and with $\hat{\nu}^{1/3} = 0.292$, 0.184 and 0.092. Despite the increasing distortion of $d_1(k)$ at large wavenumbers as $\hat{\nu} \to 0$, the effect on generation is quite small. The insensitivity of $g_1(k)$ to the value of the horizontal mixing coefficient suggests that a true enstrophy cascade connects the regions of generation and dissipation.

Fig. 8 depicts the zonal spectra of the energy generation, the energy loss due to surface drag and the loss due to lateral viscosity for two of these experiments. At $\hat{\nu}^{1/3} = 0.092$, 91% of the kinetic energy dissipation is accounted for by the surface drag, and the remainder by lateral mixing. In the wavenumber range $0 \leq k \leq 1$, over 97% of the dissipation is due to surface drag. Inspection of the two-dimensional energy spectra reveals that the feature most sensitive to these changes in $\hat{\nu}$, once again, is the sharpness of the energy peak at $(k = 0, l = 0.5)$. The sharp peak in $E(k = 0, l)$ at $l = 0.5$ when $\hat{\nu}^{1/3} = 0.292$ (Fig. 5) is replaced by a smooth maximum when $\hat{\nu}^{1/3} = 0.092$. We notice no other clearly

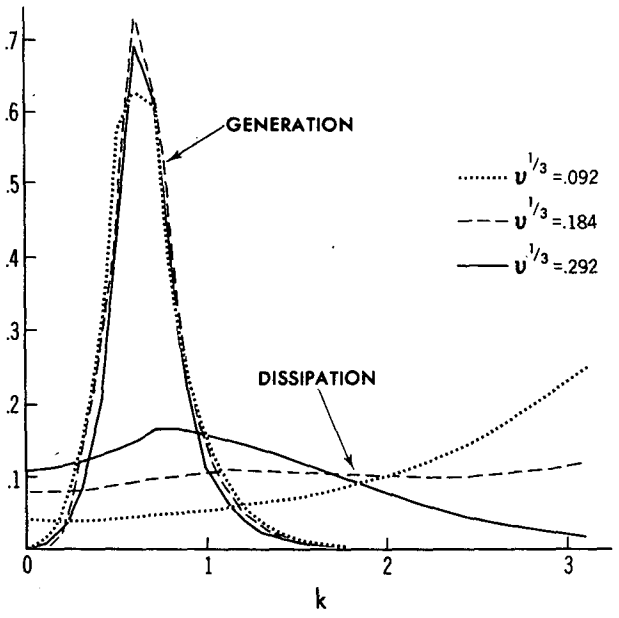

FIG. 7. Zonal spectra of potential enstrophy generation $g_1(k)$ and dissipation $d_1(k)$ in the upper layer, for experiments with $\hat{L} = 0$, $\hat{\beta} = 0.25$, $\hat{\kappa} = 0.5$, and three values of $\hat{\nu}$.

statistically significant changes in the energy-containing eddies as $\hat{\nu}^{1/3}$ is decreased to 0.092. The choice of an even lower viscosity results in a significant decrease in G (Fig. 2a). We therefore choose the $(\hat{L} = 10, \hat{\nu}^{1/3} = 0.092)$ experiment as a pivot, about which to analyze the effects of variations in $\hat{\beta}$ and $\hat{\kappa}$, believing that some distortion of the high wavenumbers is acceptable in order to obtain as inviscid a flow as possible in the energy containing eddies.

4. Pivot experiment

Having described our rationale for the choice of $(\hat{L} = 10, \hat{\nu}^{1/3} = 0.092, \hat{\beta} = 0.25, \hat{\kappa} = 0.5)$ for the pivot experiment, we discuss this simulation in more detail before proceeding.

For comparison, growth rates for the unstable modes on the time-averaged flow for these parameters are shown as a function of k and l in Fig. 9. Shaded regions in the figure are stable. The wave with the largest growth rate is $(k = 0.75, l = 0)$. For a given angle in this plane, $\phi = \tan^{-1}(l/k)$, we find that values of (k,l) which maximize the growth rate, and describe the locus of these points by a dotted line.

The time-averaged spectrum of the eddy energy generation $G(k,l)$—or equivalently, of the heat or potential vorticity flux—is contoured in Fig. 10a. The maximum generation at each angle ϕ is marked by a dash-dotted line in this figure, this line being transcribed onto Fig. 9 as well. There is considerable resemblance between the generation

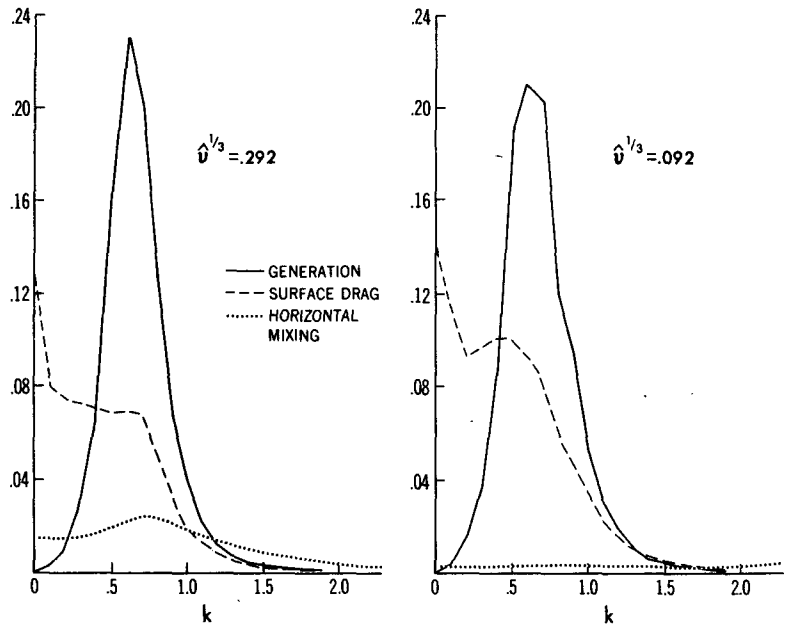

FIG. 8. Zonal spectra of eddy energy generation $G(k)$ dissipation due to surface drag $S(k)$ and dissipation due to horizontal mixing $D(k)$ for two of the experiments in Fig. 7: $\hat{\nu}^{1/3} = 0.292$ and 0.092.

spectrum and the linear growth rates. In particular, the generation has a smooth maximum near $l = 0$, and there is little generation in regions of linear stability. The generation spectrum does seem to have shifted to slightly smaller zonal wavenumbers than those with the largest linear growth rates. Larger shifts of this sort will be evident for the more energetic flows described in Section 5.

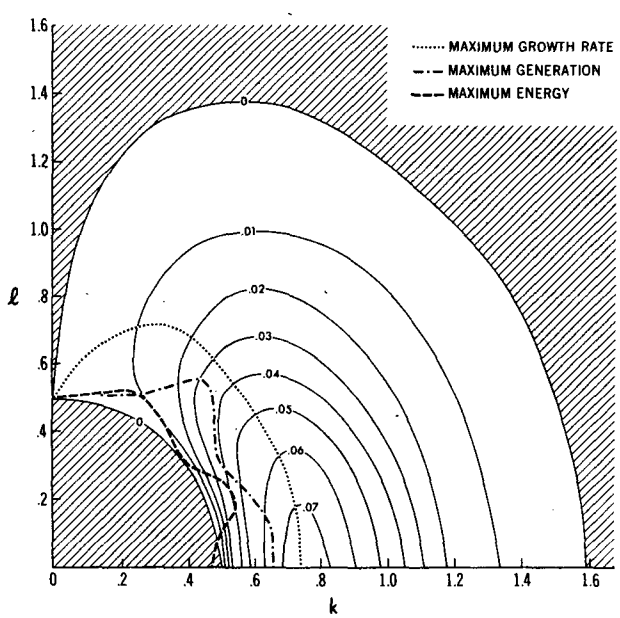

FIG. 9. Contour plot in the k-l plane of growth rate (imaginary part of complex frequency) of the unstable linear wave for $\hat{\beta} = 0.25$, $\hat{\kappa} = 0.5$, and $\hat{\nu}^{1/3} = 0.092$. The shaded region is stable. The dotted line marks the maximum growth rate at each angle $\tan^{-1}(l/k)$. The dash-dotted line marks the wave with maximum energy generation, $G(k,l)$, at each angle for the pivot experiment (see Fig. 10a). The dashed line marks the wave with maximum energy, $E(k,l)$ at each angle (see Fig. 10c).

As seen in the contoured (k-l) spectrum of nonlinear energy transfer (Fig. 10b), the net effect of nonlinear processes is to remove energy from the broad region of generation—centered near ($k = 0.7, l = 0$)—and to transfer it to motions of large zonal scale ($k = 0, l = 0.5$). The resulting (k-l) spectrum of the total eddy energy $E(k,l)$ is plotted in Fig. 10c; the wavenumber with the maximum energy at each ϕ is denoted by a dashed line in Fig. 9. The nonlinear transfer has evidently produced a reasonably isotropic energy spectrum. In addition, the energy maximum is clearly at smaller total wavenumber than the generation maximum, as one expects from the familiar two-dimensional cascade of energy to larger scales.

According to Rhines's (1975) analysis of barotropic flows on a β-plane, one expects the energy cascade from smaller to larger scales to be halted and the energy to accumulate at the total wavenumber $\mathcal{K} \equiv (\beta/V_{\text{rms}})^{1/2}$, at which the Rossby wave phase speed becomes comparable, to rms particle velocities, V_{rms}. Choosing $V_{\text{rms}} = (2E_{BT})^{1/2}$, where E_{BT} is the eddy kinetic energy in the barotropic mode (=0.83), we find $\mathcal{K} = 0.44$ for this experiment, in good agreement with Fig. 10c, which shows energy maxima along a circle of radius $\simeq 0.5$ in the (k-l) plane. The use in this argument of the baro-

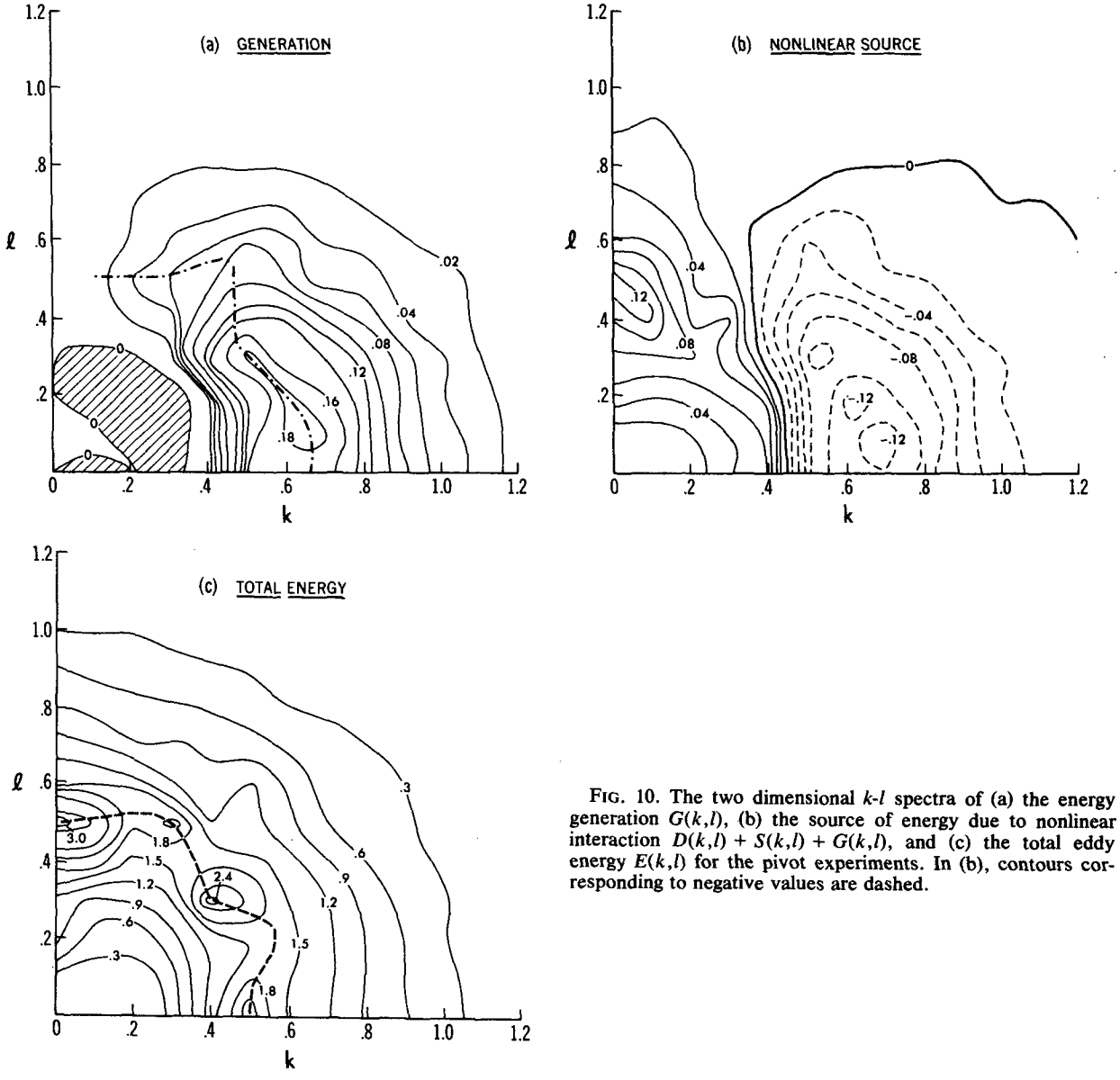

FIG. 10. The two dimensional k-l spectra of (a) the energy generation $G(k,l)$, (b) the source of energy due to nonlinear interaction $D(k,l) + S(k,l) + G(k,l)$, and (c) the total eddy energy $E(k,l)$ for the pivot experiments. In (b), contours corresponding to negative values are dashed.

tropic energy does not imply that all of the energy at this wavenumber is in the barotropic mode. The energy maximum can be created by barotropic nonlinear interactions—as described by Rhines (1977), and Salmon (1977)—but surface drag acting on these barotropic waves will generate substantial baroclinic energy as well (see Fig. 4).

5. Supercriticality and surface drag

We next consider the result obtained by varying each model parameter individually about its value in the pivot experiment. As discussed in Section 3, the effects of varying $\hat{L}$ (or k_{max}) and $\hat{\nu}$ on such global statistics as total eddy energy and energy generation are quite small, except when $\hat{L}$ is so large, or $\hat{\nu}$ so small, that the Reynolds number for the smallest wave in the system is large enough to produce severe distortion. Excluding $\hat{L}$ and $\hat{\nu}$, the parameters which remain are the nondimensional $\hat{\beta}$ (or supercriticality) and the drag $\hat{\kappa}$.

Figs. 11a and 11b show how the zonal generation (or heat flux) spectrum $G(k)$ changes as $\hat{\beta}$ is respectively decreased and increased from its pivot value. As expected from the increasing linear instability of the mean flow, G increases monotonically as $\hat{\beta}$ decreases to zero. Accompanying this increase in amplitude is a systematic shift in the spectral peak toward lower wavenumbers. In Fig. 12 we plot the wavenumber and the growth rate of the most unstable linear wave as a function of $\hat{\beta}$ and $\hat{\kappa}$ (holding $\hat{\nu}^{1/3} = 0.092$). There is a shift in the most unstable

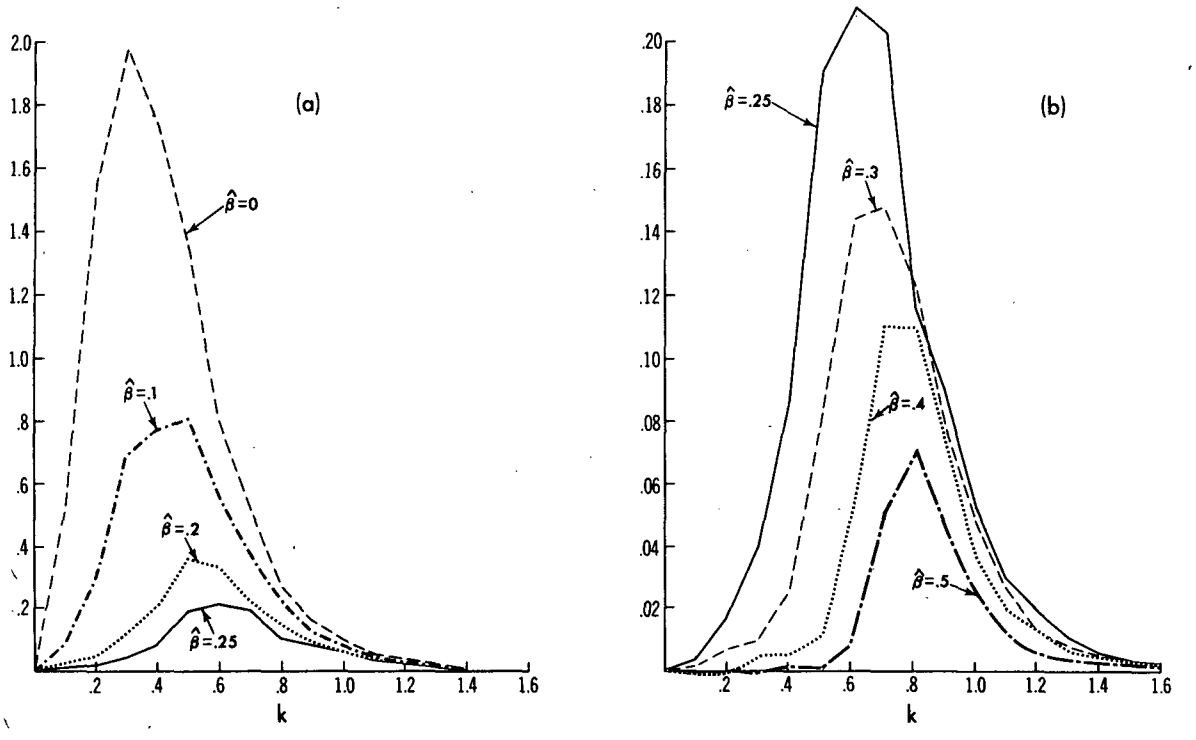

FIG. 11. The zonal spectra of energy generation $G(k)$ for experiments with $\hat{L} = 10$, $\hat{\nu}^{1/3} = 0.092$, and $\hat{\kappa} = 0.5$, and with various values of $\hat{\beta}$. Values of $\hat{\beta}$ smaller than the pivot values (0.25) are shown in (a), and values larger than the pivot value in (b). Note the order of magnitude change in scale between (a) and (b).

wavenumber—from 0.9 (at $\hat{\beta} = 0.5$, $\hat{\kappa} = 0.5$) to 0.6 (at $\hat{\beta} = 0$, $\hat{\kappa} = 0.5$)—but the magnitude of the shift is considerably smaller than that seen in Fig. 11 (from 0.8 to 0.3). As mentioned above, the nonlinear transfer of energy to larger scales should be significantly reduced when rms flow velocities become comparable to the Rossby wave phase speeds. As $\hat{\beta}$ decreases, the nonlinear transfer can be expected to carry energy to smaller wavenumbers both because of the higher energy level and because smaller $\hat{\beta}$ is associated with smaller phase speeds.

Fig. 13 shows the generation spectra for values of

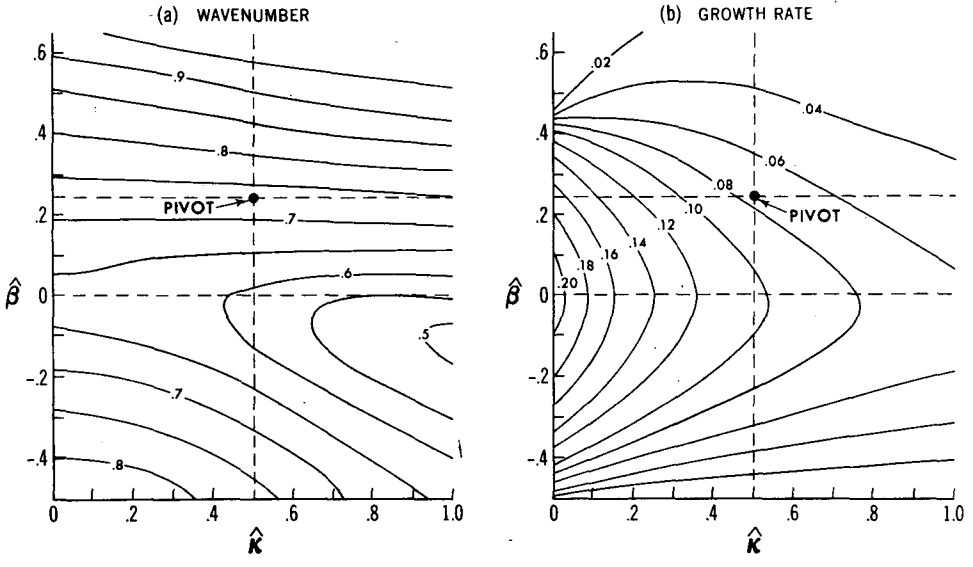

FIG. 12. (a) The zonal wavenumber and (b) the growth rate of the most unstable linear wave as a function of $\hat{\beta}$ and $\hat{\kappa}$, for $\hat{\nu}^{1/3} = 0.092$. The pivot experiment, $\hat{\beta} = 0.25$, $\hat{\kappa} = 0.5$, is denoted by a dot.

$\hat{\kappa}$ both above and below the pivot value of 0.5. Once again, the monotonic increase in generation with decreasing $\hat{\kappa}$ is consistent with the linear instability growth rates in Fig. 12. As in the $\hat{\beta}$-variation, the increase in generation is accompanied by a shift of the spectrum to longer waves. It is not possible, however, to explain this shift on the basis of linear theory; Fig. 12 shows no significant shift in the most unstable wavenumber as $\hat{\kappa}$ is varied (with $\hat{\beta} = 0.25$). As in the $\hat{\beta}$-variation, the nonlinear cascade deposits energy at larger scales when the energy level of the flow increases.

Changes in G as $\hat{\beta}$ and $\hat{\kappa}$ are varied have the same sense as changes in the growth rate of the most unstable wave ω_I. However, G cannot be thought of as a simple function of ω_I. In particular, by linearizing around the pivot experiment, one finds that similar fractional changes in $\hat{\beta}$ and $\hat{\kappa}$ have similar effects on ω_I:

$$\frac{\partial \ln \omega_I}{\partial \ln \hat{\beta}} \approx -0.88 \quad \text{and} \quad \frac{\partial \ln \omega_I}{\partial \ln \hat{\kappa}} \approx -0.62.$$

However, a fractional change in $\hat{\beta}$ clearly produces a much larger change in G than the same fractional change in $\hat{\kappa}$. Linearizing about the pivot case, we fine

$$\frac{\partial \ln G}{\partial \ln \hat{\beta}} \approx -2.3 \quad \text{and} \quad \frac{\partial \ln G}{\partial \ln \hat{\kappa}} \approx -0.46.$$

We suspect that this difference is primarily a consequence of the greater effect of $\hat{\beta}$-variation on the instability of the longer waves in which most of the energy has accumulated.

A number of additional calculations have been performed by varying both $\hat{\beta}$ and $\hat{\kappa}$ simultaneously (holding $\hat{L} = 10$, $\hat{\nu}^{1/3} = 0.092$ as before). Some properties of the resulting statistically steady states —the generation G, total eddy energy E, and the fraction of the eddy energy in the barotropic mode E_{BT}/E—are summarized in $\hat{\beta}$-$\hat{\kappa}$ plane diagrams in Fig. 14. An attempt to obtain results for ($\hat{\beta} = 0$, $\hat{\kappa} = 0.2$) proved unsuccessful; the energy increased to such an extent that the small time step required for numerical stability made the calculation impractical. If a statistically steady-state exists, it apparently has an order of magnitude more eddy energy than ($\hat{\beta} = 0$, $\hat{\kappa} = 0.5$). In the absence of the stabilizing effect of $\hat{\beta}$ on the larger scales to which the energy cascades, the generation and energy level increase much more rapidly with decreasing $\hat{\kappa}$.

In contrast, at $\hat{\beta} = 0.4$ there is a slight decrease in G as $\hat{\kappa}$ decreases from 0.5 to 0.2. Theories for weakly unstable dissipative flows (Pedlosky, 1970) predict a time-averaged generation or heat flux proportional to $\hat{\kappa}$. The result for $\hat{\beta} = 0.4$ may signal a shift to this characteristic behavior of weakly unstable flows from the (totally different) behavior

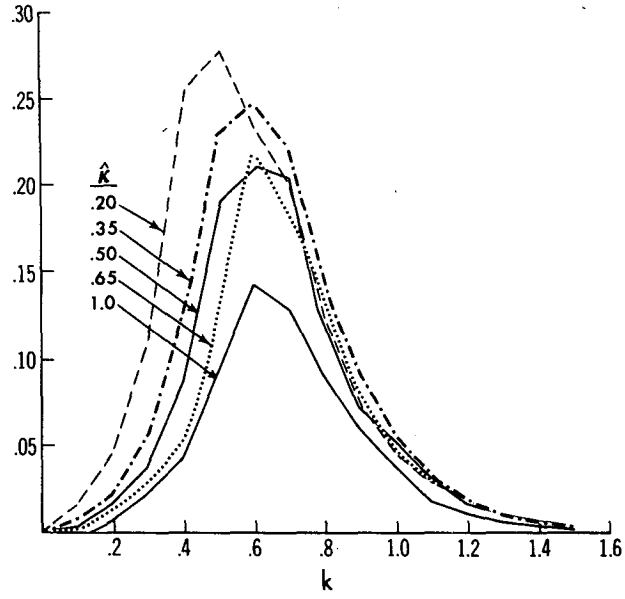

FIG. 13. The zonal spectra of the energy generation $G(k)$ for experiments with $\hat{L} = 10$, $\hat{\nu}^{1/3} = 0.092$, $\hat{\beta} = 0.25$, and various values of $\hat{\kappa}$.

exhibited by the strongly nonlinear flows at smaller $\hat{\beta}$.

As indicated in the figures, one experiment has also been conducted with negative $\hat{\beta}$ (temperature decreasing equatorward). Comparing the two cases with ($|\hat{\beta}| = 0.1$, $\hat{\kappa} = 0.5$), we find that negative $\hat{\beta}$ results in the more energetic flow. If $\hat{\kappa}$ were zero, these two cases would of necessity be equally energetic, as can be seen from a simple symmetry argument. [The model equations are invariant under the transformation $\hat{\beta} \rightarrow -\hat{\beta}$ and (level 1) $\leftrightarrow$ (level 2) if $\hat{\kappa} \equiv 0$.] But as Fig. 12b indicates, the presence of $\hat{\kappa}$ breaks this symmetry and results in larger growth rates for $\hat{\beta} = -0.1$ than for $\hat{\beta} = +0.1$.

The barotropic fraction of the eddy energy (Fig. 14c) has a very well-defined behavior in the $\hat{\beta}$-$\hat{\kappa}$ plane. It clearly decreases with increasing $\hat{\kappa}$, but is independent of $\hat{\beta}$ to a surprising degree. We can offer no explanation for this simple behavior. Experiments with unequal depth layers (listed in Appendix B) suggest that the barotropic energy fraction depends on the ratio of the layer depths (δ) as well as $\hat{\kappa}$.

For those points in the $\hat{\beta}$-$\hat{\kappa}$ plane far removed from the pivot experiment, it is not clear that the dependence on $\hat{L}$ and $\hat{\nu}$ is at all similar to that described in Section 3. It is not clear, in particular, that all the results in Fig. 14 are nearly independent of $\hat{L}$ and $\hat{\nu}$. In fact, we find in some experiments with $\hat{\beta} = 0.25$, $\hat{\kappa} = 0.167$, and $\hat{L} = 15$, that the dependence of the flow statistics on $\hat{\nu}$ is much stronger than for $\hat{\kappa} = 0.5$, even for $\hat{\nu}$ sufficiently large that the finite resolution should not be a factor (experiments 30–32 in Appendix B). However, the changes in G

and E in the $\hat{\beta}$-$\hat{\kappa}$ plane (Figs. 14a and 14b) are considerably larger than changes in the $\hat{L}$-$\hat{\nu}$ plane (Figs. 2a,b). We suspect, therefore, that the same qualitative behavior would be obtained in a model with greater resolution, in which one could obtain $\hat{L}$- and $\hat{\nu}$-independent results in a larger portion of the $\hat{\beta}$-$\hat{\kappa}$ plane.

6. Eddy heat flux parameterization

In the limit in which the mean flow is nearly constant over the distance λ, the results described in Section 3—particularly those summarized in Figs. 3–6—offer some evidence that the eddy statistics are dependent on the local mean flow only, and not on the meridional extent of the unstable region (nor, presumably, on other global properties of the flow). Accepting the existence of this "homogeneous limit" and ignoring possible distortion of the results due to inadequate resolution, the parameter variations discussed in Section 5 show how the eddy statistics in this "homogeneous limit" depend on the mean flow properties. By fitting a smooth function to the results in Fig. 14a, for example, it is possible to obtain a preliminary estimate of the relation

$$G = G(\hat{\beta},\hat{\kappa}) = \lim_{\hat{\nu}\to 0}\lim_{\hat{L}\to\infty}\lim_{k_{\max}\to\infty} G(\hat{\beta},\hat{\kappa},\hat{L},\hat{\nu},k_{\max}) \quad (8)$$

for the nondimensional eddy energy generation per unit mass. [The limits in Eq. (8) are not entirely interchangeable; as noted in Section 3, one cannot let $\hat{\nu}\to 0$ at fixed $k_{\max}$.] For the dimensional energy generation, G_*, this gives

$$G_* = U^3\lambda^{-1}G(\hat{\beta},\hat{\kappa}), \quad (9)$$

U being the difference in mean velocity between the two layers. G_* is also equal to the generation of eddy available potential energy in this homogeneous problem; therefore, the dimensional eddy buoyancy flux

$$B_* \equiv \tfrac{1}{2}g'\overline{(v_1 + v_2)\eta}$$

(where η denotes the displacement of the interface from its mean position) can be expressed in terms of G:

$$B_* = -4f_0\lambda^2U^{-1}G_* = -4U^2\lambda f_0G(\hat{\beta},\hat{\kappa}). \quad (10)$$

If we define a diffusivity $\mathscr{D}$ such that

$$B_* = -\mathscr{D}g'\partial\bar{\eta}/\partial y = -\mathscr{D}Uf_0,$$

then

$$\mathscr{D} \equiv 4U\lambda G(\hat{\beta},\hat{\kappa}). \quad (11)$$

If the factor $G(\hat{\beta},\hat{\kappa})$ were a constant, this diffusivity could be thought of as a product of a "mixing length" proportional to λ and a "mixing speed" proportional to U. Eq. (10) would then reduce to the closure suggested by Stone (1972).

The concept of an eddy diffusivity $\mathscr{D}$ is particularly useful for estimating the penetration length—the distance to which the effects of eddy fluxes on the mean flow penetrate meridionally into an unstable region (see Fig. 1b). If the mean flow relaxes to its (unstable) equilibrium values on the time scale τ, then we expect the mean flow to be affected by the eddies in a boundary layer of thickness $\gamma \approx (\mathscr{D}\tau)^{1/2}$. Using (11) we have

$$\gamma \approx 2(\lambda U\tau G)^{1/2} = 2\lambda(G\tau/\tau_A)^{1/2}, \quad (12)$$

where $\tau_A \equiv \lambda/U$ is the advective time scale.

We focus now on the dependence of B_* on the mean horizontal and vertical density "gradients", holding g, f_0 and H fixed. The horizontal gradient of the vertically-averaged density,

$$\frac{(\rho_2 - \rho_1)}{2H}\frac{\partial\bar{\eta}}{\partial y} \equiv \Delta_y$$

is, then, proportional to U, while the density difference in the vertical,

$$\rho_2 - \rho_1 \equiv H\Delta_z$$

is proportional to λ^2. Therefore,

$$B_* \propto \Delta_y^2\Delta_z^{1/2}G(\hat{\beta},\hat{\kappa}).$$

Perturbing Δ_y and Δ_z, noting that $\hat{\beta} \propto \Delta_z\Delta_y^{-1}$ and $\hat{\kappa} \propto \Delta_z^{1/2}\Delta_y^{-1}$ yields

$$\frac{\partial \ln B_*}{\partial \ln\Delta_y} = 2 - \frac{\partial \ln G}{\partial \ln\hat{\beta}} - \frac{\partial \ln G}{\partial \ln\hat{\kappa}},$$

$$\frac{\partial \ln B_*}{\partial \ln\Delta_z} = \frac{1}{2} + \frac{\partial \ln G}{\partial \ln\hat{\beta}} + \frac{1}{2}\frac{\partial \ln G}{\partial \ln\hat{\kappa}}.$$

Using the (Section 5) values around the pivot experiment,

$$\frac{\partial \ln B_*}{\partial \ln\Delta_y} \approx 2 + 2.3 + 0.46 \approx 4.8,$$

$$\frac{\partial \ln B_*}{\partial \ln\Delta_z} \approx \tfrac{1}{2} - 2.3 - 0.23 \approx -2.0.$$

The variations in $\hat{\kappa}$ have a small (10%) effect on the fluxes. The variations in $\hat{\beta}$, in contrast, enhance the heat flux sensitivity to Δ_y by more than a factor of 2 and change the sign of the response to perturbations in Δ_z. Held (1978) finds similar results by analyzing sensitivity experiments with a two-layer primitive equation atmospheric model. Fig. 14 suggests, however, that $\hat{\kappa}$-variations grow in importance as $\hat{\beta}$ and $\hat{\kappa}$ decrease.

The dimensional potential vorticity fluxes in upper and lower layers can also be written in terms of G,

$$\overline{v_1'q_1'} = -\overline{v_2'q_2'} = -2G_*U^{-1} = -2U^2\lambda^{-1}G(\hat{\beta},\hat{\kappa})$$

$$= -\frac{2U\lambda\beta}{\hat{\beta}}G(\hat{\beta},\hat{\kappa})$$

$$= -\frac{\beta}{2\hat{\beta}}\mathscr{D}.$$

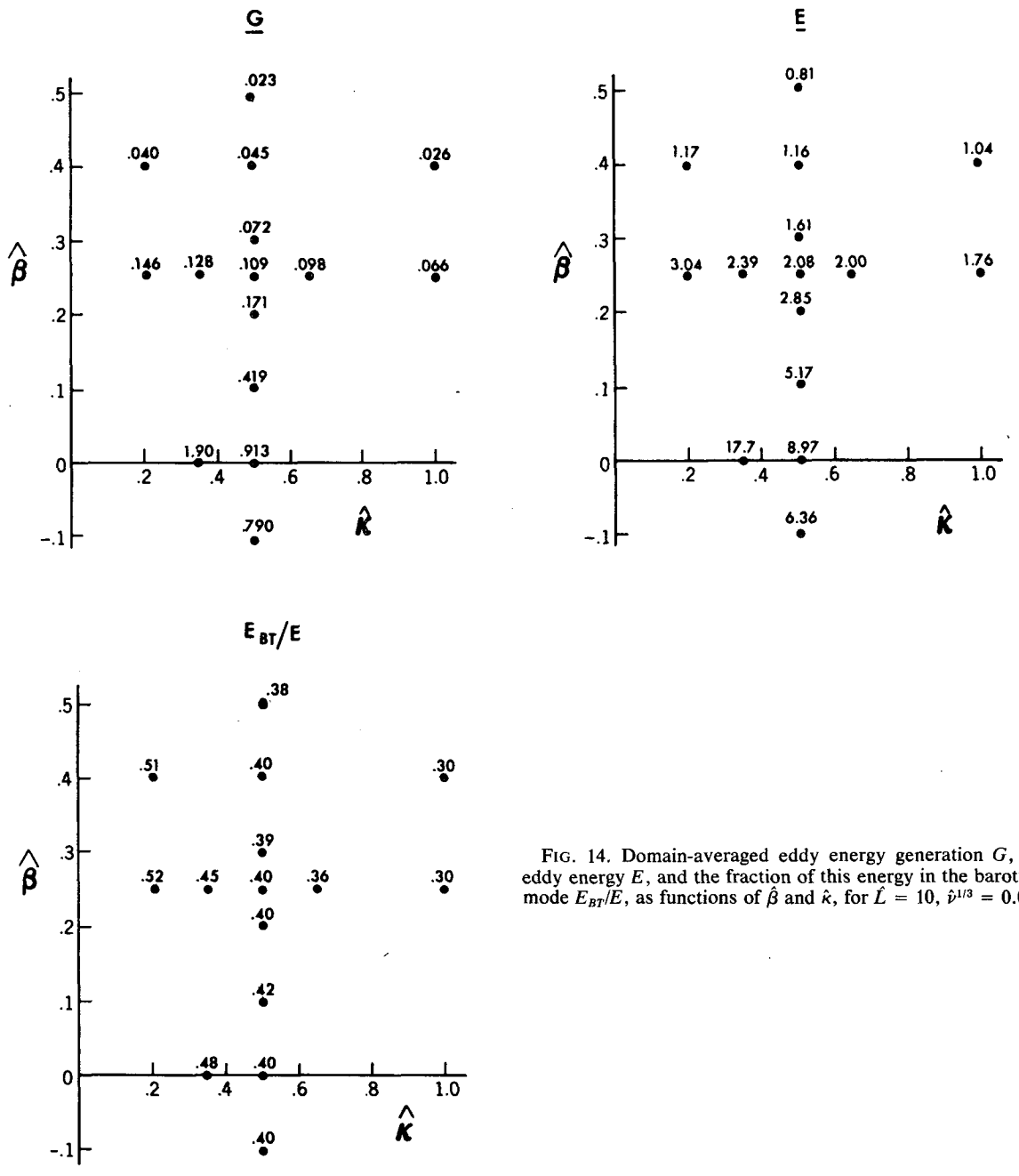

FIG. 14. Domain-averaged eddy energy generation G, total eddy energy E, and the fraction of this energy in the barotropic mode E_{BT}/E, as functions of $\hat{\beta}$ and $\hat{\kappa}$, for $\hat{L} = 10$, $\hat{\nu}^{1/3} = 0.092$.

Knowledge of the transient eddy potential vorticity fluxes is generally required in order to solve for the time mean potential vorticity and, therefore, for the time mean geostrophic flow. If all dissipative and diabatic terms are linear, so that non-conservative effects do not introduce any additional coupling between the transients and the mean, then the eddy potential vorticity fluxes in the two layers are, in fact, all one needs to know about the transients in order to compute the mean flow. In this simple case, $G(\hat{\beta},\hat{\kappa})$ is the only transient statistic needed for closure in the homogeneous limit.

7. Concluding remarks

Assuming that the time-mean flow in the two-layer quasi-geostrophic model on a beta-plane is a horizontally uniform vertical shear, the equations for the evolution of deviations from this mean flow can be integrated numerically in a doubly periodic domain. The resulting statistically steady state is horizontally homogeneous within the model domain. We have examined the dependence of this statistically steady state on various model parameters and have found, in a particular parameter range, that the

eddy statistics do not change significantly as the size of the doubly periodic domain is increased, holding fixed all other parameters. Being nearly independent of domain size, we suspect that the results are also nearly independent of boundary conditions and, therefore, that essentially the same homogeneous statistically steady state would be obtained whenever the forces driving the unstable flow are characterized by sufficiently large horizontal scales. The existence of this "homogeneous limit" in the two-layer quasi-geostrophic model makes the turbulent closure problem in this model fundamentally different from the closure problem in three-dimensional shear flows and in turbulent Bénard convection.

We have attempted a preliminary description of the dependence of various eddy statistics of interest on the model parameters. A number of questions have been left unanswered, each of which suggests directions in which these results can be extended. We list some of these directions:

- While our results suggest that the eddy statistics are independent of the size of the domain $\hat{L}$ if $\hat{L}$ is sufficiently large and if the model's numerical resolution is adequate, our choice of experiments has not resulted in a very precise definition of the model's behavior in the $\hat{\nu}$-$\hat{L}$ plane (Fig. 2). The extent to which the $\hat{\beta}$-$\hat{\kappa}$ plane results depend on the values of $\hat{\nu}$ and $\hat{L}$ should certainly be examined more carefully before any quantitative results are taken seriously.
- In the $\hat{\beta}$-$\hat{\kappa}$ plane, the limit $\hat{\beta} \to \hat{\beta}_M$, where $\hat{\beta}_M$ is the minimum value of $\hat{\beta}$ required to stabilize the mean flow, is of particular interest. The extent to which these homogeneous results can be understood in terms of weakly non-linear theory when $\hat{\beta}$-$\hat{\beta}_M$ is small is deserving of careful analysis.
- The model provides a simple framework in which to study the generation of transient zonal jets in a baroclinically unstable environment. Our pivot experiment does not, unfortunately, provide a particularly good example of this phenomenon, its energy spectrum being rather isotropic. Several other of our experiments produce much more anisotropic spectra, dominated by a peak at $k = 0$ and $l = l_E \neq 0$. What determines l_E, the characteristic meridional scale of these jets? Is it determined by the energy level of the flow (Rhines, 1975; Williams, 1978), or by the radius of deformation, at least in weakly nonlinear cases in which one may be able to think of these jets as generated by secondary baroclinic instability (Pedlosky, 1975)? We have not obtained a sufficient variety of experiments with zonal jets of sharply defined meridional scale to address this point.
- By concentrating on wavenumber spectra, we have neglected other ways of describing the results. Analysis of frequency spectra, in particular, would allow one to compare the characteristic phase speed of disturbances with the predictions of linear theory (and also help one estimate the sampling errors in the computation of mean statistics). Casual inspection of the flow field in several experiments indicates that a surprising amount of energy is in disturbances that move very slowly with respect to the lower layer flow.
- There are other qualitative features of the flow in physical space that are difficult to analyze in a spectral representation. Flow fields in some experiments are dominated by more or less isolated vortices. In other experiments the eddies seem to be organized into wave packets, each packet consisting of more or less the same number of wavelengths of the dominant wave. Some experiments show a filamentary structure in the vorticity fields similar to that often observed in two-dimensional turbulence simulations, while other experiments do not exhibit this characteristic structure. How one would make a precise analysis of these various physical space features is unclear.
- In oceanic applications of the two-layer model, one generally chooses a shallow upper layer and deep lower layer. While a few statistically steady states with unequal layer depths have been obtained (see Appendix B), the dependence of the eddy statistics on the ratio of layer depths has not been investigated systematically.
- Neither have we considered problems in which the planetary vorticity gradient and mean temperature gradient are not parallel (or anti-parallel). The direction as well as the magnitude of the heat or potential vorticity flux vector is needed for closure in these more general problems.

It will undoubtedly be difficult to find an environment in the atmosphere sufficiently homogeneous for a theory valid in the homogeneous limit to be directly applicable (not to mention the problem of applying results from a two-layer model). Finding an application in the oceanic interior seems more likely, though still far from certain. Yet one can still hope that an asymptotic theory valid in the limit $(\lambda/L) \to 0$ may be of qualitative value even when $(\lambda/L) \approx 1$ (as is often the case with WKB–like approximations).

Independent of any possibility of immediate practical application, we believe these results are of interest for several theoretical reasons:

1) The homogeneous results and theory can be used to test proposed parameterization schemes. These schemes should at least reduce to the correct theory in the limit $(\lambda/L) \to 0$.

2) The computation of the eddy flux in this homogeneous problem can be attempted with turbulent closure schemes of varying sophistication (e.g.,

Salmon, 1980), thus providing a point of contact between work on parameterizing atmospheric and oceanic eddy fluxes and work on homogeneous turbulence.

3) Using one's understanding of the local homogeneous theory, one can hope to construct systematically a weakly nonlocal theory as the next term in an asymptotic expansion in (λ/L).

Acknowledgments. Funding and computational resources for this work were provided to one of the authors (DBH) by the National Science Foundation through Grant OCE78-25700 and the National Center for Atmospheric Research. The figures were drafted by the Scientific Illustration Group at the Geophysical Fluid Dynamics Laboratory/NOAA. This paper is Contribution No. 4553 of the Woods Hole Oceanographic Institution and No. 129 of the POLYMODE program.

APPENDIX A

Notation for Spectra

Using (5), the eddy kinetic energy density in the ith layer, for example, becomes

$$K_i = \frac{1}{(2\pi\hat{L})^2}\int \tfrac{1}{2}(u_i^2 + v_i^2)dxdy$$

$$= \sum_{m=-N/2}^{N/2-1}\sum_{n=-N/2}^{N/2-1} K^i_{mn},$$

with

$$K^i_{mn} \equiv \tfrac{1}{2}(k_m^2 + l_n^2)|A_{mn}|^2.$$

The reality of ψ implies that $|A^i_{-m,-n}|^2 = |A^i_{mn}|^2$ so

$$K_i = 2\sum_{m=0}^{N/2} c_m \sum_{n=-N/2}^{N/2-1} K^i_{mn}$$

$$= 2\sum_{m=0}^{N/2}\sum_{n=0}^{N/2} c_m c_n (K^i_{mn} + K^i_{m,-n}),$$

where

$$c_m = \begin{cases} \tfrac{1}{2}, & \text{if } m = 0 \text{ or } m = N/2 \\ 1, & \text{otherwise.} \end{cases}$$

If $\psi_i(x,y,t)$ is a solution to (2), then $\psi_i(x, -y,t)$ is also a solution. These solutions must have the same statistics, assuming that there is only one statistically steady state with non-zero probability of evolving from random initial conditions. Therefore $|A_{m,n}|^2 = |A_{m,-n}|^2$ and $K^i_{mn} = K^i_{m,-n}$. (It follows from this symmetry argument that the time-averaged meridional flux of zonal momentum is identically zero.) We therefore define the two-dimensional spectrum,

$$K_i(k_m,l_n) = 2\hat{L}^2[K^i_{mn} + K^i_{m,-n}],$$

so that

$$K_i = \hat{L}^{-2}\sum_{m=0}^{N/2}\sum_{n=0}^{N/2} c_m c_n K_i(k_m,l_n).$$

In the limit of infinite resolution, then,

$$K_i = \int_0^\infty \int_0^\infty dk\, dl\, K_i(k,l)$$

since $\Delta k = \Delta l = \hat{L}^{-1}$. One-dimensional spectra are defined by

$$K_i(k) = \hat{L}^{-1}\sum_{n=0}^{N/2} c_n K_i(k,l_n),$$

$$K_i(l) = \hat{L}^{-1}\sum_{m=0}^{N/2} c_m K_i(k_m,l),$$

so that

$$K_i = \hat{L}^{-1}\sum_{m=0}^{N/2} c_m K_i(k_m) = \hat{L}^{-1}\sum_{n=0}^{N/2} c_n K_i(l_n).$$

In order to avoid too elaborate a notation, we use the same symbol K_i to refer to the domain average, the two-dimensional spectrum $K_i(k,l)$, and both the one-dimensional spectra, $K(k)$ and $K(l)$; the intended meaning is always clear from the context. Spectra of the other quantities discussed in the text are defined analogously.

APPENDIX B

Table of Numerical Experiments

All of the statistically steady states analyzed are listed in the following table. Several of these are not discussed in the text, including some with the ratio of layer depths, $\delta \equiv H_1/H_2$, not equal to unity. When $\delta \neq 1$ the radius of deformation is defined to be $\lambda^2 = g'H_1H_2/[f_0^2(H_1 + H_2)]$, and the energy in the barotropic mode is

$$E_{BT} = \left\langle \frac{1}{2}\left|\nabla\left(\frac{H_1\psi_1 + H_2\psi_2}{H_1 + H_2}\right)\right|^2 \right\rangle.$$

($\delta = 1$ unless otherwise specified in the table.) Listed in the table are the following:

E	total eddy energy
$E(k = 0)$	total eddy energy in the $k = 0$ mode
p	total potential enstrophy $[=p_1 + p_2]$
$p(k = 0)$	total potential enstrophy in $k = 0$ mode
G	eddy energy generation
E_{BT}/E	fraction of energy in the barotropic mode
S/D	ratio of energy dissipation due to surface drag to that due to horizontal viscosity
k_E	the *nonzero* zonal wavenumber at which $E(k)$ attains its maximum value
k_G	the zonal wavenumber at which $G(k)$ attains its maximum value
l_E	the meridional wavenumber at which $E(k = 0, l)$ attains its maximum value. (An asterisk implies that this maximum is sharp, no other values of l having as much as half the energy of the indicated wavenumber.)

All quantities in the table are nondimensional.

TABLE B1. Table of numerical experiments.

Exp. no.	$\hat{L}$	$\hat{\beta}$	$\hat{\kappa}$	$\hat{\nu}^{1/3}$ × 10	δ	E	E (k = 0)	p	p (k = 0)	G	E_{BT}/E	S/D	k_E	k_G	l_E
1	7	0.25	0.5	0.645		2.20	2.56	13.5	10.9	0.112	0.394	20.0	3/7	4/7	3/7
2	7	0.25	0.5	0.921		1.94	2.02	10.7	8.54	0.101	0.389	14.8	3/7	4/7	3/7
3	7	0.25	0.5	1.84		1.86	1.11	9.24	9.10	0.101	0.359	5.35	3/7	4/7	3/7
4	7	0.25	0.5	2.92		1.50	1.85	7.14	7.34	0.087	0.327	2.26	3/7	5/7	(2, 4)/7
5	10	−0.1	0.5	0.921		6.36	7.12	39.3	30.2	0.785	0.401	20.3	0.3	0.4	0.1
6	10	0.0	0.35	0.921		17.7	21.4	100.0	73.0	1.94	0.477	16.5	0.2	0.2	0.3
7	10	0.0	0.5	0.921		8.97	8.90	54.4	37.2	0.913	0.402	16.3	0.2	0.3	0.3
8	10	0.1	0.5	0.921	0.25	2.49	2.46	40.0	30.4	0.094	0.156	8.90	0.4, 0.5	0.5	0.5
9	10	0.1	0.5	0.921		5.17	5.76	32.2	24.0	0.419	0.418	13.1	0.3	0.5	0.5
10	10	0.167	0.5	0.921	0.50	2.40	2.22	23.3	15.6	0.119	0.267	9.38	0.4, 0.5	0.6	0.5
11	10	0.2	0.5	0.921		2.85	2.98	17.6	12.9	0.171	0.402	11.0	0.5	0.5	0.5
12	10	0.25	0.167	0.691		4.19	4.64	26.6	15.6	0.183	0.566	11.0	0.4	0.5	0.3
13	10	0.25	0.167	1.38		2.95	7.24	12.0	16.6	0.139	0.535	7.21	0.4	0.4	0.3*
14	10	0.25	0.2	0.921		3.04	4.08	15.8	12.5	0.146	0.523	9.85	0.4	0.5	0.4
15	10	0.25	0.35	0.921		2.39	2.28	14.2	9.46	0.128	0.449	10.1	0.5	0.6	0.6
16	10	0.25	0.5	0.461		2.03	1.36	25.1	9.64	0.075	0.470	11.7	0.6	0.6	0.8
17	10	0.25	0.5	0.921		2.08	2.89	12.9	12.2	0.109	0.397	10.0	0.5	0.6	0.5
18	10	0.25	0.5	1.38		2.08	2.40	10.9	9.60	0.112	0.376	7.35	0.5	0.6	0.5*
19	10	0.25	0.5	1.84		1.87	2.46	9.31	9.44	0.104	0.366	5.10	0.4, 0.5	0.6	0.5*
20	10	0.25	0.5	2.92		1.66	1.45	7.82	11.1	0.098	0.334	2.36	0.5	0.6	0.5*
21	10	0.25	0.65	0.921		2.00	1.78	12.6	8.50	0.098	0.364	10.1	0.4, 0.5	0.6	0.6
22	10	0.25	1.0	0.921		1.76	2.04	10.9	9.86	0.067	0.304	9.54	0.5	0.6	0.7*
23	10	0.3	0.5	0.921		1.61	1.90	10.0	8.30	0.072	0.392	9.14	0.6	0.7	0.5
24	10	0.4	0.167	1.38		1.01	4.82	4.73	14.2	0.035	0.517	4.91	0.6	0.7	0.4*
25	10	0.4	0.2	0.921		1.17	5.28	6.50	17.1	0.040	0.511	7.57	0.6	0.7	0.6
26	10	0.4	0.5	0.921		1.16	3.06	7.48	12.3	0.045	0.398	7.76	0.6, 0.7	0.7, 0.8	0.5*
27	10	0.4	1.0	0.921		1.04	2.90	6.44	13.0	0.026	0.301	7.28	0.6	0.7	0.4, 0.6
28	10	0.5	0.5	0.921		0.814	2.25	5.11	9.72	0.023	0.367	6.50	0.1	0.8	0.6*
29	15	0.0	0.5	1.38		6.38	6.81	39.6	29.8	0.607	0.411	7.37	1/15	6/15	3/15
30	15	0.25	0.167	1.38		3.56	4.83	18.5	13.9	0.175	0.564	4.21	5/15	8/15	4/15
31	15	0.25	0.167	2.76		2.12	6.60	8.13	15.9	0.113	0.487	2.23	(1, 6)/15	8/15	6/15*
32	15	0.25	0.167	5.52		0.901	2.20	3.58	6.02	0.071	0.394	0.552	1/15	9/15	5/15
33	15	0.25	0.5	0.731		1.06	0.63	11.6	4.52	0.038	0.486	5.62	9/15	10/15	12/15
34	15	0.25	0.5	0.921		1.37	0.96	12.3	5.82	0.060	0.468	5.10	8/15	10/15	(6–9)/15
35	15	0.25	0.5	1.38		1.66	2.01	10.6	9.04	0.091	0.416	4.38	(7, 8)/15	(9–11)/15	7/15
36	15	0.25	0.5	2.92		1.62	1.35	7.69	7.25	0.095	0.329	2.19	7/15	11/15	7/15*
37	15	0.4	0.167	1.38		0.874	5.46	4.84	16.3	0.031	0.536	3.15	9/15	12/15	7/15*

REFERENCES

Bretherton, F. P., and D. B. Haidvogel, 1976: Two-dimensional turbulence above topography. *J. Fluid Mech.*, **78**, 129–154.

Haltiner, G. J., 1971: *Numerical Weather Prediction*. Wiley, 317 pp.

Held, I. M., 1978: The tropospheric lapse rate and climatic sensitivity: Experiments with a two-level atmospheric model. *J. Atmos. Sci.*, **35**, 2083–2098.

Holland, W. R., 1978: The role of mesoscale eddies in the general circulation of the ocean: Numerical experiments using a wind-driven quasi-geostrophic model. *J. Phys. Oceanogr.*, **8**, 363–392.

Orszag, S. A., 1971: Numerical simulation of incompressible flows within simple boundaries. I. Galerkin (spectral) representations. *Stud. Appl. Math.*, **50**, 293–327.

Pedlosky, J., 1963: Baroclinic instability in two layer systems. *Tellus*, **15**, 20–25.

——, 1970: Finite-amplitude baroclinic waves. *J. Atmos. Sci.*, **27**, 15–30.

——, 1975: On secondary baroclinic instability and the meridional scale of motion in the ocean. *J. Phys. Oceanogr.*, **5**, 603–607.

Phillips, N. A., 1951: A simple three-dimensional model for the study of large-scale extratropical flow patterns. *J. Meteor.*, **8**, 381–394.

Rhines, P. B., 1975: Waves and turbulence on a β-plane. *J. Fluid Mech.*, **69**, 417–443.

——, 1977: The dynamics of unsteady currents. Vol. 6, *Marine Modelling, The Sea*, E. D. Goldberg, I. N. McCane, J. J. O'Brien, and J. H. Steele, Eds., Wiley, 189–318.

Salmon, R., 1977: Two-layer quasigeostrophic turbulence in a simple special case. *Geophys. Astrophys. Fluid Dyn.*, **10**, 25–52.

——, 1980: Baroclinic instability and geostrophic turbulence. *Geophys. Astrophys. Fluid Dyn.*, **15**, 167–211.

Simmons, A. J., 1974: The meridional scale of baroclinic waves. *J. Atmos. Sci.*, **31**, 1515–1525.

Stone, P. H., 1972: A simplified radiative-dynamical model for the static stability of rotating atmospheres. *J. Atmos. Sci.*, **29**, 405–418.

Tennekes, H., and J. L. Lumley, 1972: *A First Course in Turbulence*. The MIT Press, 300 pp.

Williams, G. P., 1978: Planetary circulations: 1. Barotropic representation of Jovian and terrestrial turbulence. *J. Atmos. Sci.*, **35**, 1399–1426.